

Using White Dish CMB Anisotropy Data to Probe Open and Flat- Λ CDM Cosmogonies

Bharat Ratra¹, Ken Ganga², Naoshi Sugiyama³, G. S. Tucker⁴, G. S. Griffin⁵, H. T. Nguyen⁶,
and J. B. Peterson⁵

Received _____; accepted _____

¹Department of Physics, Kansas State University, Manhattan, KS 66506.

²IPAC, MS 100–22, California Institute of Technology, Pasadena, CA 91125.

³Department of Physics, Kyoto University, Kitashirakawa-Oiwakecho, Sakyo-ku, Kyoto 606.

⁴Department of Physics, Brown University, Box 1843, Providence, RI 02912.

⁵Physics Department, Carnegie Mellon University, 5000 Forbes Avenue, Pittsburgh, PA 15213.

⁶Jet Propulsion Laboratory, California Institute of Technology, Pasadena, CA 91109.

ABSTRACT

We use data from the White Dish experiment to set limits on cosmic microwave background radiation anisotropies in open and spatially-flat- Λ cold dark matter cosmogonies. We account for the White Dish calibration uncertainty, and marginalize over the offset and gradient removed from the data. Our $2\text{-}\sigma$ upper limits are larger than those derived previously. These upper limits are consistent with those derived from the *COBE*-DMR data for all models tested.

Subject headings: cosmic microwave background—cosmology: observations—large-scale structure of the universe

1. Introduction

Ganga et al. (1997a, hereafter GRGS) developed techniques to account for uncertainties, such as those in the beamwidth and calibration, in likelihood analyses of cosmic microwave background (CMB) anisotropy data. GRGS and Ganga et al. (1997b,1998) used these techniques, in conjunction with theoretical CMB anisotropy spectra, in analyses of the UCSB South Pole 1994 (Gundersen et al. 1995), the SuZIE (Church et al. 1997), and the MAX 4+5 (Tanaka et al. 1996; Lim et al. 1996, and references therein) CMB anisotropy data sets. Bond & Jaffe (1997) have also analyzed the UCSB South Pole 1994 data and the Saskatoon (Netterfield et al. 1997) data.

In this paper we present a similar analysis of the Tucker et al. (1993, hereafter T93) White Dish CMB anisotropy data collected at the South Pole. The White Dish detector and telescope are described in Tucker et al. (1994). Data were taken in a frequency band centered at 90 GHz. The FWHM of the beam, assumed to be gaussian, is $12'$. Five interlocked circles on the sky, centered at constant elevation and declination, were observed. The circle centers are separated by $15'$ on the sky, and each circle intersects at least one neighbour at two points. The circles, of diameter $28'$ on the sky, were sampled at 128 equally spaced points. Griffin et al. (1997) describe the full White Dish data set.

T93 analyze a small subset of the White Dish data in two different ways, which they refer to as Method I and Method II. They consider only the set of points, at two different elevations, defined by where the interlocking circles intersect. Method I uses two sets of two-beam temperature differences (one set at each elevation). Method II uses a single set of “quadrupole” temperature differences, obtained by appropriately combining the corresponding two-beam differences at each elevation. Further details are given in T93.

Neither method results in a $2\text{-}\sigma$ detection of CMB anisotropy (T93). Since Method II provides a less restrictive upper limit than does Method I, we do not record Method II results here. Method I and Method II use essentially the same CMB anisotropy observations; they thus can not be combined to provide a tighter upper limit. T93 remove an offset and linear gradient from each

Method I scan, prior to binning in right ascension.

T93 and Tucker et al. (1994) describe how White Dish was calibrated. The absolute calibration uncertainty is 30% ($1-\sigma$).

In §2 we briefly summarize the computational techniques used in our analysis. See GRGS for further details. Results are presented and discussed in §3, and conclusions are given in §4.

2. Summary of Computation

Figure 1 shows the reduced White Dish Method I data.

For two White Dish circles centered at azimuth angles ϕ_i and ϕ_j , the Method I window function is

$$W_{lij} = e^{-\sigma_G^2(l+0.5)^2} \times \left[2P_l \left(\cos \left\{ \sqrt{\Delta\theta^2 + (\phi_i - \phi_j)^2} \right\} \right) - P_l \left(\cos \left\{ \sqrt{\Delta\theta^2 + (\phi_i - \phi_j - \Delta\phi)^2} \right\} \right) - P_l \left(\cos \left\{ \sqrt{\Delta\theta^2 + (\phi_i - \phi_j + \Delta\phi)^2} \right\} \right) \right]. \quad (1)$$

Here the gaussian beamwidth $\sigma_G = 12'/\sqrt{8\ln 2}$, P_l is a Legendre polynomial of order l (the multipole), the throw $\Delta\phi = 15'$, and the separation in elevation $\Delta\theta$ is zero for two points at the same elevation and is $23.6'$ for two points at different elevations.

We do not record results from the Method II analysis here. However, since the Method II window function has not been given in the published literature, we note that it is

$$W_{lij} = e^{-\sigma_G^2(l+0.5)^2} \times \left[2P_l (\cos \{\phi_i - \phi_j\}) - 0.5P_l (\cos \{\phi_i - \phi_j - \Delta\phi\}) - 0.5P_l (\cos \{\phi_i - \phi_j + \Delta\phi\}) + 0.5P_l \left(\cos \left\{ \sqrt{\Delta\theta^2 + (\phi_i - \phi_j - \Delta\phi)^2} \right\} \right) + 0.5P_l \left(\cos \left\{ \sqrt{\Delta\theta^2 + (\phi_i - \phi_j + \Delta\phi)^2} \right\} \right) - P_l \left(\cos \left\{ \sqrt{\Delta\theta^2 + (\phi_i - \phi_j)^2} \right\} \right) \right], \quad (2)$$

where the notation is the same as that for equation (1), except $\Delta\theta$ is always $23.6'$ here. The zero-lag parts of the Method I and II window functions are shown in Figure 2 and the window function parameters are given in Table 1.

Figure 2 also shows some of the model CMB anisotropy spectra we use. These spectra are described in Ratra et al. (1997). In addition to the flat bandpower and fiducial cold dark matter (CDM) model spectra, we consider spatially open CDM models as well as spatially flat CDM models with a cosmological constant (Λ). The low-density open and flat- Λ models are consistent with most current observations. See Bunn & White (1997), Górski et al. (1998), Gott (1997), Turner (1997), Peacock (1997), Cole et al. (1997), and Gardner et al. (1997) for discussions.

The computation of the CMB anisotropy spectra is described in Sugiyama (1995). These computations assume gaussian⁷, adiabatic primordial energy density power spectra. The open model computations assume the open-bubble inflation model energy-density spectrum (Ratra & Peebles 1994,1995; Bucher, Goldhaber, & Turok 1995; Yamamoto, Sasaki, & Tanaka 1995). The flat- Λ model computations assume the scale-invariant energy-density power spectrum (Harrison 1970; Peebles & Yu 1970; Zel'dovich 1972).

The CMB anisotropy spectra are parameterized by their quadrupole-moment amplitude $Q_{\text{rms-PS}}$, the clustered-mass density parameter Ω_0 , the baryonic-mass density parameter Ω_B , and the Hubble parameter $h [= H_0/(100h \text{ km s}^{-1} \text{ Mpc}^{-1})]$. The cosmological parameter values tested were chosen on the basis of consistency with current non-CMB observations (Ratra et al. 1997). Table 2 shows the parameter values used in our analyses.

Figure 3 shows the moments $(\delta T_{\text{rms}}^2)_l = T_0^2(2l+1)C_l W_l/(4\pi)$ (where T_0 is the CMB

⁷It has recently been suggested that degree-scale CMB anisotropy observations might indicate nongaussianity (Gaztañaga, Fosalba, & Elizalde 1997). In this case, the good fit of gaussian models to the data, indicated by very low reduced χ^2 values for some models (Ganga, Ratra, & Sugiyama 1996, also see Lineweaver & Barbosa 1997), would be a coincidence. As would the almost identical conclusions deduced from the UCSB South Pole 1994 and MAX 4+5 data sets (Ganga et al. 1998).

temperature now, GRGS, eqs. [5] & [6]) for the Method I window function and the CMB anisotropy spectra of Figure 2. These moments show the angular scales where the Method I experiment is most sensitive, given a CMB anisotropy model (GRGS). Examination of the White Dish window function by itself (i.e., without reference to a CMB anisotropy spectrum) does not give an accurate indication of the multipoles to which the experiment is sensitive (Table 1 and Figure 2).

The computation of the likelihood function is described in GRGS. We assume a uniform prior in the amplitudes of the offset and gradient removed and marginalize over these amplitudes, i.e., we integrate over all possible offset and gradient amplitudes when determining the likelihood function (Bond et al. 1991, also see Bunn et al. 1994; GRGS; Church et al. 1997; Ganga et al. 1997b). Calibration uncertainty is accounted for as described in GRGS. Figure 4 shows the Method I likelihood functions for the CMB anisotropy spectra of Figure 2. These likelihood functions account for all the above additional uncertainties.

In agreement with the conclusion of T93, there are no $2\text{-}\sigma$ detections of anisotropy (defined using the prescription given in GRGS). To derive $Q_{\text{rms-PS}}$ upper limits we assume a uniform prior in $Q_{\text{rms-PS}}$ and integrate the posterior probability density distribution function starting from $0\text{ }\mu\text{K}$ until 95.5% of the area is encompassed. This is the $2\text{-}\sigma$ highest posterior density (HPD) prescription; see GRGS for further details. (The corresponding $2\text{-}\sigma$ equal tail limits, e.g., GRGS, are significantly larger and so not recorded here.) Table 2 gives these $Q_{\text{rms-PS}}$ $2\text{-}\sigma$ HPD limits, as well as those for bandtemperature $\delta T_l = \delta T_{\text{rms}} / [\sum_{l=2}^{\infty} [(l+0.5)W_l / \{l(l+1)\}]]^{0.5}$.

3. Results and Discussion

From Table 2, the Method I δT_l $2\text{-}\sigma$ upper limit for the flat bandpower angular spectrum is $150\text{ }\mu\text{K}$. This accounts for the marginalization over the amplitudes of the offset and gradient removed, as well as the calibration uncertainty. If instead we use a gaussian autocorrelation function (GACF), with a coherence angle of 0.15° , to describe the CMB anisotropy, the

corresponding bandtemperature δT_l limit is $140 \mu\text{K}$, in good agreement with the flat bandpower angular spectrum result. Ignoring the marginalization over offset and gradient removed, and the calibration uncertainty, the flat bandpower δT_l $2\text{-}\sigma$ upper limit is $54 \mu\text{K}$. Accounting only for the marginalization over offset and gradient, the flat bandpower δT_l $2\text{-}\sigma$ limit rises to $96 \mu\text{K}$. These numerical values should be compared to the T93 bandtemperature δT_l $2\text{-}\sigma$ upper limit of $44 \mu\text{K}$, derived for a GACF with a coherence angle of 0.15° . The T93 computation does not account for calibration uncertainty, nor does it account for the marginalization over the amplitudes of the offset and gradient removed from the data.

The White Dish Method I limits derived here are larger than that of T93. The Method II upper limits (not recorded here) are larger than those of Method I. This is in qualitative agreement with the results of T93. For all models tested, the White Dish $Q_{\text{rms-PS}}$ $2\text{-}\sigma$ upper limits derived here are consistent with the DMR detections (Górski et al. 1996,1998; Stompor 1997).

The limits derived depend sensitively on whether offset and gradient removal are accounted for in the likelihood analysis, and whether calibration uncertainty is included. There are situations in which the calibration uncertainty need not be included (for example, when considering the ratio of two different measurements made with the same instrument). For comparison with other experiments, however, calibration uncertainty must be included.

The variation of the δT_l upper limit from model to model gives an indication of the accuracy of the flat bandpower approximation. From Table 2 we see that there is a difference of $\sim 20\%$ between the two extreme cases. This is comparable to the $\sim 25\%$ difference for SuZIE (Ganga et al. 1997b), and larger than the $\sim 10\%$ variation for UCSB South Pole 1994 and MAX 4+5 (GRGS; Ganga et al. 1998).

4. Conclusion

In our likelihood analyses of the White Dish Method I CMB anisotropy data we have marginalized over the amplitudes of the offset and gradient removed from the data, and have

explicitly accounted for calibration uncertainty. There are no $2\text{-}\sigma$ detections of anisotropy for the models tested, in agreement with the conclusion of T93. As a consequence of the additional effects accounted for here, the limits we have derived are less restrictive than those derived by T93. These limits are consistent with the *COBE*-DMR anisotropy amplitudes for the models tested. Hence, contrary to earlier assertions (e.g., Ostriker & Steinhardt 1995; Ratra et al. 1997), the T93 White Dish data subset does not seriously constrain cosmological parameter values for reasonable DMR-normalized models.

We acknowledge helpful discussions with J. Gundersen, L. Page, and G. Rocha. BR acknowledges support from NSF grant EPS-9550487 with matching support from the state of Kansas and from a K*STAR First award. This work was partially carried out at the Infrared Processing and Analysis Center and the Jet Propulsion Laboratory of the California Institute of Technology, under a contract with the National Aeronautics and Space Administration.

Table 1: Numerical Values for the Zero-Lag Window Function Parameters^a

	$l_{e^{-0.5}}$	l_e	l_m	$l_{e^{-0.5}}$	$\sqrt{I(W_l)}$
Method I	297	477	539	825	1.18
Method II	415	579	615	833	0.725

^aThe value of l where W_l is largest, l_m , the two values of l where $W_{l_{e^{-0.5}}} = e^{-0.5}W_{l_m}$, $l_{e^{-0.5}}$, the effective multipole, $l_e = I(lW_l)/I(W_l)$, and $I(W_l) = \sum_{l=2}^{\infty} (l+0.5)W_l/\{l(l+1)\}$.

Table 2: Upper Limits^a on $Q_{\text{rms-PS}}$ and δT_l (in μK) from the Method I Analysis

#	$(\Omega_0, h, \Omega_B h^2)$	$Q_{\text{rms-PS}}$	δT_l
O1	(0.1, 0.75, 0.0125)	72	150
O2	(0.2, 0.65, 0.0175)	70	150
O3	(0.2, 0.70, 0.0125)	75	150
O4	(0.2, 0.75, 0.0075)	81	150
O5	(0.3, 0.60, 0.0175)	66	160
O6	(0.3, 0.65, 0.0125)	72	160
O7	(0.3, 0.70, 0.0075)	77	150
O8	(0.4, 0.60, 0.0175)	63	160
O9	(0.4, 0.65, 0.0125)	67	160
O10	(0.4, 0.70, 0.0075)	71	160
O11	(0.5, 0.55, 0.0175)	54	170
O12	(0.5, 0.60, 0.0125)	57	170
O13	(0.5, 0.65, 0.0075)	61	160
O14	(1.0, 0.50, 0.0125)	59	170
$\Lambda 1$	(0.1, 0.90, 0.0125)	71	170
$\Lambda 2$	(0.2, 0.80, 0.0075)	68	170
$\Lambda 3$	(0.2, 0.75, 0.0125)	64	170
$\Lambda 4$	(0.2, 0.70, 0.0175)	61	170
$\Lambda 5$	(0.3, 0.70, 0.0075)	63	170
$\Lambda 6$	(0.3, 0.65, 0.0125)	59	170
$\Lambda 7$	(0.3, 0.60, 0.0175)	56	180
$\Lambda 8$	(0.4, 0.65, 0.0075)	61	170
$\Lambda 9$	(0.4, 0.60, 0.0125)	57	170
$\Lambda 10$	(0.4, 0.55, 0.0175)	54	180
$\Lambda 11$	(0.5, 0.60, 0.0125)	57	170
Flat	...	97	150

^a2- σ (95.5%) HPD limits.

REFERENCES

- Bond, J.R., Efstathiou, G., Lubin, P.M., & Meinhold, P.R. 1991, *Phys. Rev. Lett.*, 66, 2179
- Bond, J.R., & Jaffe, A. 1997, in *Microwave Background Anisotropies*, ed. F.R. Bouchet, R. Gispert, B. Guiderdoni, & J. Tran Thanh Van (Gif-sur-Yvette: Editions Frontieres), 197
- Bucher, M., Goldhaber, A.S., & Turok, N. 1995, *Phys. Rev. D*, 52, 3314
- Bunn, E.F., & White, M. 1997, *ApJ*, 480, 6
- Bunn, E., White, M., Srednicki, M., & Scott, D. 1994, *ApJ*, 429, 1
- Church, S.E., Ganga, K.M., Ade, P.A.R., Holzapfel, W.L., Mauskopf, P.D., Wilbanks, T.M., & Lange, A.E. 1997, *ApJ*, 484, 523
- Cole, S., Weinberg, D.H., Frenk, C.S., & Ratra, B. 1997, *MNRAS*, 289, 37
- Ganga, K., Ratra, B., & Sugiyama, N. 1996, *ApJ*, 461, L61
- Ganga, K., Ratra, B., Gundersen, J.O., & Sugiyama, N. 1997a, *ApJ*, 484, 7 (GRGS)
- Ganga, K., Ratra, B., Church, S.E., Sugiyama, N., Ade, P.A.R., Holzapfel, W.L., Mauskopf, P.D., & Lange, A.E. 1997b, *ApJ*, 484, 517
- Ganga, K., Ratra, B., Lim, M.A., Sugiyama, N., & Tanaka, S.T. 1998, *ApJS*, 114, in press
- Gardner, J.P., Katz, N., Weinberg, D.H., & Hernquist, L. 1997, *ApJ*, 486, 42
- Gaztañaga, E., Fosalba, P., & Elizalde, E. 1997, *ApJ*, submitted
- Górski, K.M., Banday, A.J., Bennett, C.L., Hinshaw, G., Kogut, A., Smoot, G.F., & Wright, E.L. 1996, *ApJ*, 464, L11
- Górski, K.M., Ratra, B., Stompor, R., Sugiyama, N., & Banday, A.J. 1998, *ApJS*, 114, 1
- Gott III, J.R. 1997, in *Critical Dialogues in Cosmology*, ed. N. Turok (Singapore: World Scientific), in press
- Griffin, G.S., Nguyễn, H.T., Peterson, J.B., & Tucker, G.S. 1997, in preparation
- Gundersen, J.O., et al. 1995, *ApJ*, 443, L57

- Harrison, E.R. 1970, *Phys. Rev. D*, 1, 2726
- Lim, M.A., et al. 1996, *ApJ*, 469, L69
- Lineweaver, C.H., & Barbosa, D. 1997, *ApJ*, submitted
- Netterfield, C.B., Devlin, M.J., Jarosik, N., Page, L., & Wollack, E.J. 1997, *ApJ*, 474, 47
- Ostriker, J.P., & Steinhardt, P.J. 1995, *Nature*, 377, 600
- Peacock, J.A. 1997, *MNRAS*, 284, 885
- Peebles, P.J.E., & Yu, J.T. 1970, *ApJ*, 162, 815
- Ratra, B., & Peebles, P.J.E. 1994, *ApJ*, 432, L5
- Ratra, B., & Peebles, P.J.E. 1995, *Phys. Rev. D*, 52, 1837
- Ratra, B., Sugiyama, N., Banday, A.J., & Górski, K.M. 1997, *ApJ*, 481, 22
- Stompor, R. 1997, in *Microwave Background Anisotropies*, ed. F.R. Bouchet, R. Gispert, B. Guiderdoni, & J. Tran Thanh Van (Gif-sur-Yvette: Editions Frontieres), 91
- Sugiyama, N. 1995, *ApJS*, 100, 281
- Tanaka, S.T., et al. 1996, *ApJ*, 468, L81
- Tucker, G.S., Griffin, G.S., Nguyễn, H.T., & Peterson, J.B. 1993, *ApJ*, 419, L45 (T93)
- Tucker, G.S., Peterson, J.B., Netterfield, C.B., Griffith, E.L., & Griffin, G.S. 1994, *Rev. Sci. Instrum.*, 65, 301
- Turner, M. S. 1997, in *Critical Dialogues in Cosmology*, ed. N. Turok (Singapore: World Scientific), in press
- Yamamoto, K., Sasaki, M., & Tanaka, T. 1995, *ApJ*, 455, 412
- Zel’dovich, Ya.B. 1972, *MNRAS*, 160, 1P

Figure Captions

Fig. 1.— Measured thermodynamic temperature differences (with $\pm 1\text{-}\sigma$ error bars) on the sky as a function of scan position. The triangles correspond to the + elevation scans of T93 and the circles correspond to the – elevation scans.

Fig. 2.— CMB anisotropy multipole moments $l(l+1)C_l/(2\pi) \times 10^{10}$ (broken lines, scale on left axis) as a function of multipole l , for selected open models O2, O12, and O14 (fiducial CDM), flat- Λ models $\Lambda 4$, $\Lambda 11$, and Flat (bandpower), normalized to the DMR maps (Górski et al. 1996,1998; Stompor 1997). See Table 2 for model-parameter values. Also shown are the White Dish Method I and II zero-lag window functions W_l (solid lines, scale on right axis). See Table 1 for W_l -parameter values.

Fig. 3.— $(\delta T_{\text{rms}}^2)_l$ as a function of l , for the Method I window function, and for the selected model spectra shown in Figure 2. These curves should be compared to the Method I window function shown in Figure 2. Note the multiple “sensitivity” peaks for some of the spectra. Note also that these peaks correspond to a different angular scale in each of the models.

Fig. 4.— Method I likelihood functions for the six CMB anisotropy spectra of Figure 2.

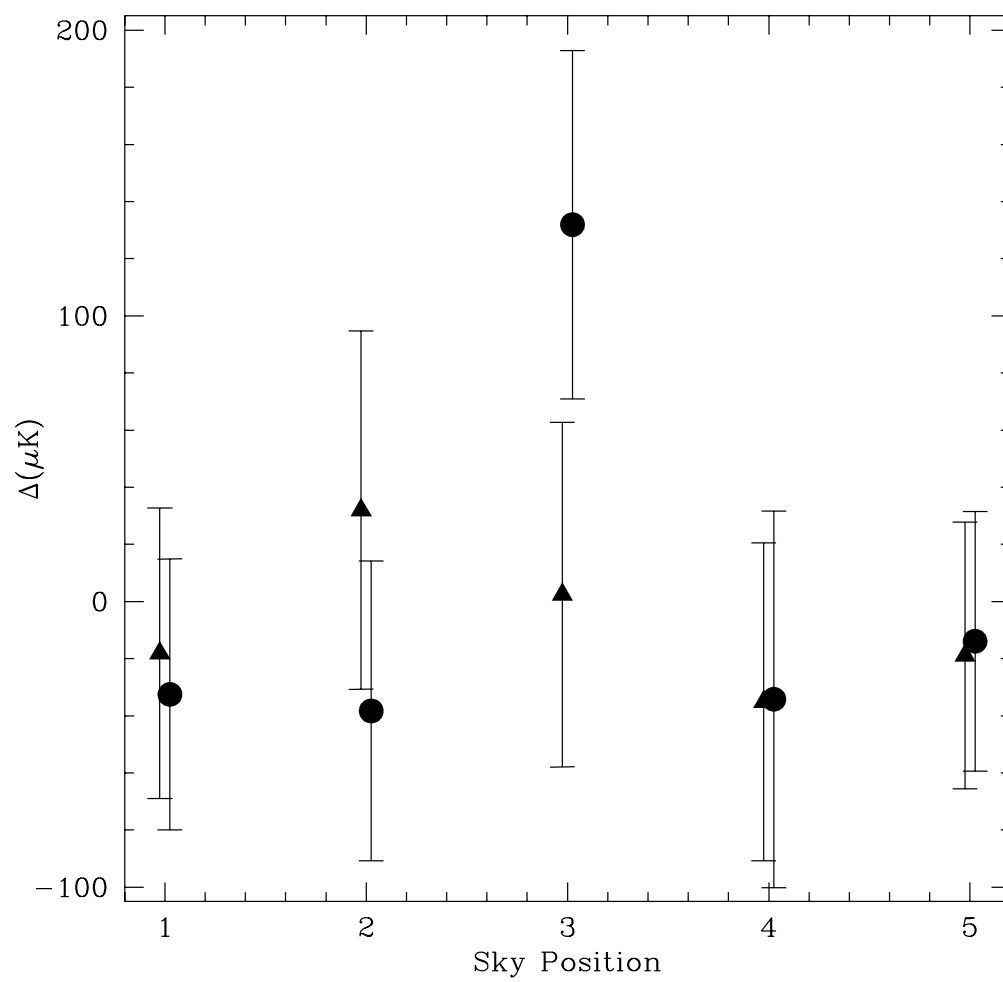


Figure 1

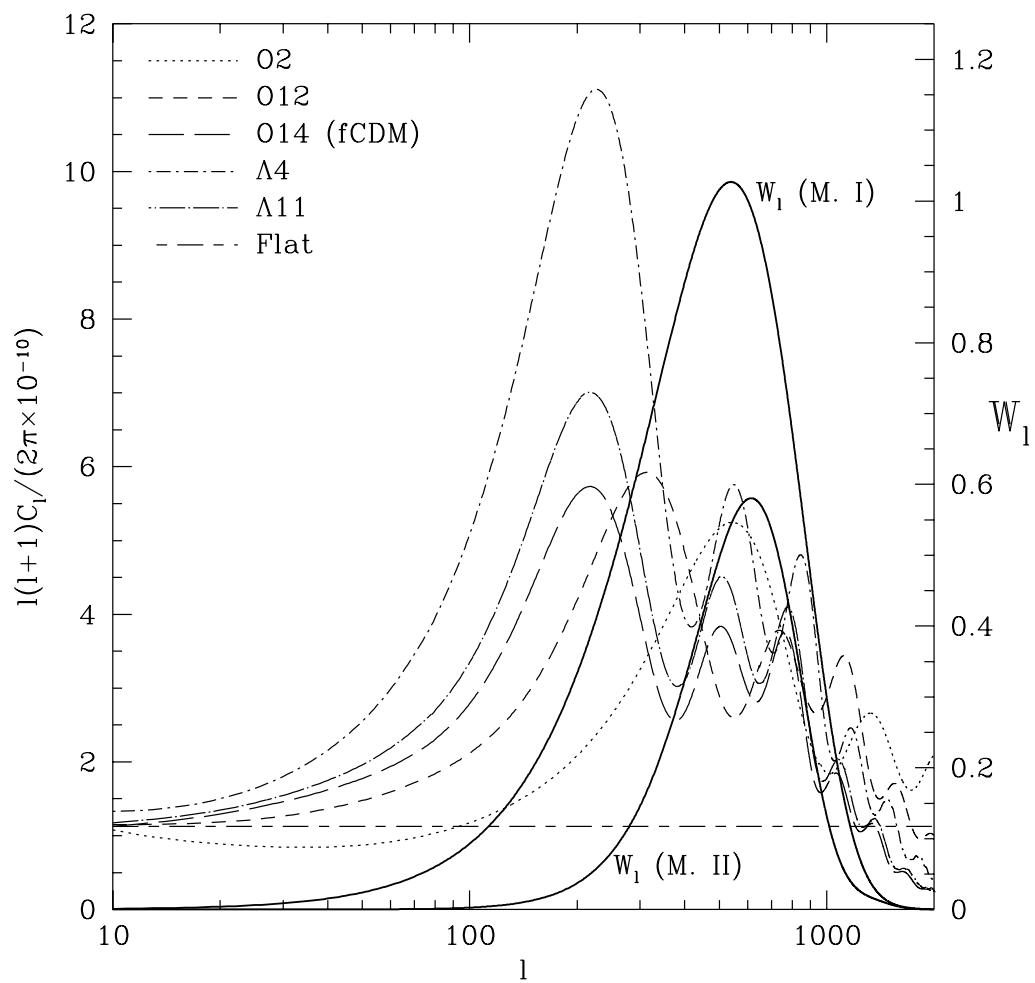


Figure 2

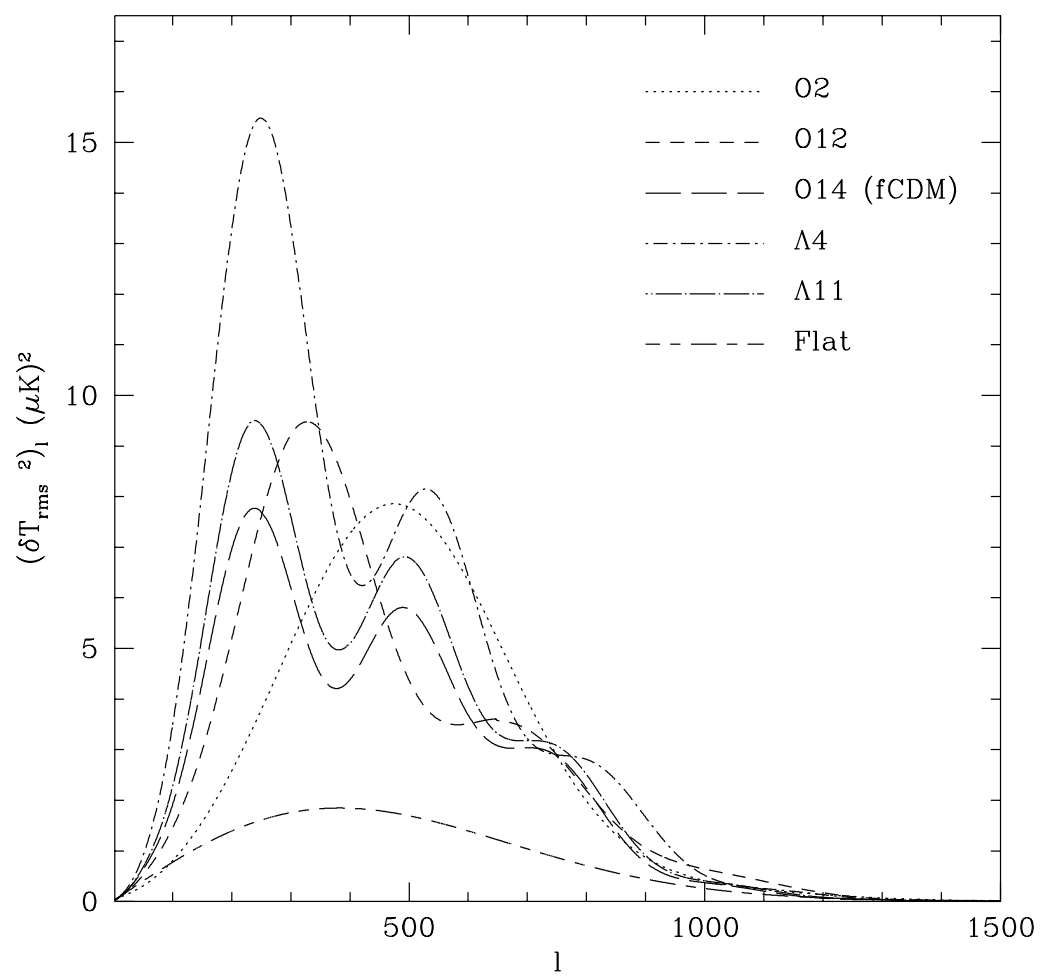


Figure 3

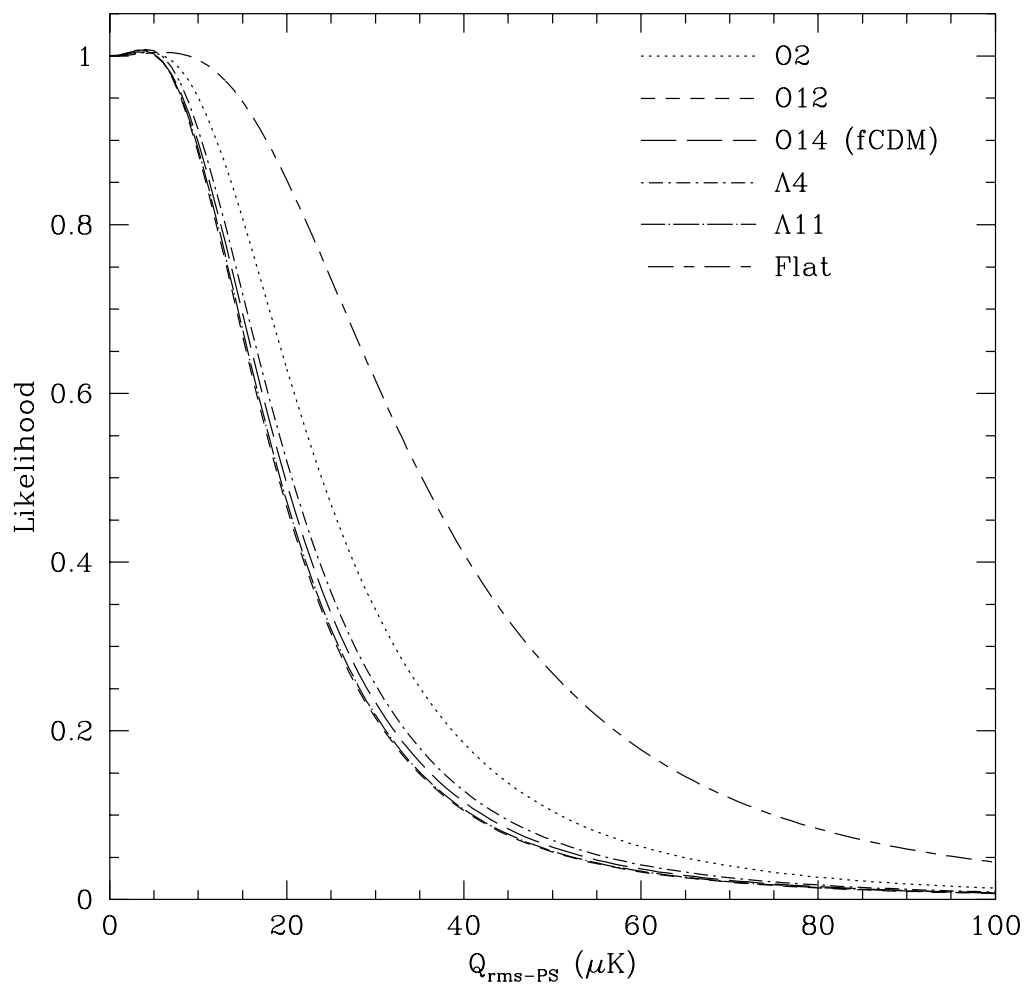


Figure 4